Carbohydrate Polymers 291 (2022) 119517

Contents lists available at ScienceDirect

Carbohydrate Polymers

journal homepage: www.elsevier.com/locate/carbpol

Design of heat sealable starch-chitosan bioplastics reinforced with reduced graphene oxide for active food packaging

Zélia Alves, PhD [a,b], Nuno M. Ferreira, PhD [c], Paula Ferreira, PhD [a,*], Cláudia Nunes, PhD [a,*]

[a] CICECO - Aveiro Institute of Materials, Department of Materials and Ceramic Engineering, University of Aveiro, 3810-193 Aveiro, Portugal
[b] CICECO - Aveiro Institute of Materials, Department of Chemistry, University of Aveiro, 3810-193 Aveiro, Portugal
[c] i3N, Department of Physics, University of Aveiro, 3810-193 Aveiro, Portugal

ARTICLE INFO

Keywords:
Bionanocomposites
Blend
Antioxidant activity
Sealing
Electrical conductivity

ABSTRACT

Interest in producing films from renewable and biodegradable polymers, such as polysaccharides, has increased in recent years with the aim of reducing the environmental pollution caused by petroleum-based plastics. Additionally, combining the thermoplastic property of starch with the antioxidant and antimicrobial activities of chitosan is of great interest to develop active materials for food packaging. This study aims the preparation of thermoplastic blended starch-chitosan films mechanically reinforced with reduced graphene oxide (rGO). Blending the starch with chitosan and rGO showed that films had a hydrophobic surface (>100°), low water solubility (weight loss less than 10%), and improved antioxidant activity. Furthermore, blended film prepared with 75% starch and 25% chitosan with rGO achieved the maximum value of electrical conductivity (6.51×10^{-3} S/m) while maintaining the heat sealing properties of starch. The functional properties and heat sealability of starch-chitosan blended films with rGO enhance their application for active food packaging.

1. Introduction

New trends in the packaging sector have been explored, namely the substitution of petroleum-based plastics by other ones with more environmentally friendly impacts. Therefore, a promising and sustainable alternative option for a food packaging material includes natural biopolymers due to their biodegradability properties, satisfying the current environmental challenges (Ghanbarzadeh et al., 2015; Kabir et al., 2020). Among them, polysaccharides extracted from abundant renewable resources have been extensively investigated, such as starch, chitosan, alginate, and/or cellulose (Ferreira et al., 2016).

Starch, a natural polymer used as a storage energy compound by the plants, is one of the most abundant polysaccharides with good film-forming properties, low cost and non-toxicity, making it a good candidate for food packaging material (Mose & Maranga, 2011). Usually, commercial starch is extracted mostly from corn, cassava, maize, potato, and rice by-products. This polysaccharide is composed of two macromolecules, amylose and amylopectin, with a widely varying ratio depending on the botanical source. The ratio difference of both macromolecules is responsible for distinct processing conditions and final properties of the films formed, including thermal, mechanical, barrier, where in general a higher amylose content increases all the above-mentioned properties (Copeland et al., 2009; Ojogbo et al., 2020). A great advantage of starch as a competitive polymer is its thermoplastic ability in the presence of water and/or a plasticizer (e.g. glycerol) with a heat treatment, allowing the starch granules gelatinization (Zhang et al., 2014). The thermoplastic ability allows the starch to be processed by various industrial processing technologies, including extrusion (Vedove et al., 2021), injection (Weerapoprasit & Prachayawarakorn, 2016), and compression molding (Ceballos et al., 2020). In addition, the starch-based films can be heat sealed to produce sachets or bags for food packaging. However, fragility, poor mechanical properties, and hydrophilicity are some drawbacks that should be overcome (Thakur et al., 2019). These properties can be improved by different modifications, for instance through the blending of two or more polymers (Hasan et al., 2020; Junlapong et al., 2019) and also with the addition of active and reinforcing agents (Gürler & Torğut, 2020; Nzenguet et al., 2018). Blending starch with degradable polymers, such as poly(lactic acid) (Chotiprayon et al., 2020), poly(ε-caprolactone) (Nevoralová et al., 2020) or polyvinyl alcohols (Kong et al., 2020), has been successful to enhance the mechanical and thermal properties. Recently, other natural biopolymers like chitosan have also received growing attention (Ren et al., 2017; Suriyatem et al., 2018). Chitosan is, similarly to starch, a polysaccharide with non-toxicity, biodegradability, biocompatibility,

* Corresponding authors.
E-mail addresses: zeliaralves@ua.pt (Z. Alves), nmferreira@ua.pt (N.M. Ferreira), pcferreira@ua.pt (P. Ferreira), claudianunes@ua.pt (C. Nunes).

https://doi.org/10.1016/j.carbpol.2022.119517
Received 24 November 2021; Received in revised form 6 April 2022; Accepted 19 April 2022
Available online 30 April 2022

and with film-forming properties. Obtained mostly from the exoskeleton of crustaceans, chitosan is the second polysaccharide most abundant in nature and has inherent bioactive properties that include antimicrobial and antioxidant activities, important features to be imparted for an active food packaging material (Haghighi et al., 2020; Wang et al., 2020). Although the enormous potential of chitosan, the lack of heat sealability limits its application as a packaging material and the blending with a thermoplastic polymer (e.g., starch) is an alternative to circumvent this limitation.

Heat sealability, which consists of binding two layers of films by pressing them between two heated plates for some time, is one of the important criteria that polymeric films should have to be further applied at an industrial scale as a packaging material (Das & Chowdhury, 2016). Additionally, a set of factors including the composition, surface molecular structure, thickness, and melting temperature of the films, allied to the seal treatment conditions (impulse time, jaw pressure, and dwell time), are responsible to affect the heat sealability and the final seal strength, which is an indication of seal quality (Lim et al., 2020). Blending starch and chitosan is a simple and cost-effective strategy to improve the mechanical and barrier properties of films produced by solvent casting (Ren et al., 2017; Zheng et al., 2019), but very little information is available about films' heat sealing properties. The effect of different ratios of chitosan and starch on the seal strength properties of blended films is not known.

The performance and applications of starch-chitosan blended films would certainly benefit from the incorporation of reinforcing agents which impart to the matrix new functionalities, such as electrical conductivity properties. In fact, the production of biodegradable material with good electrical conductivity may be a good strategy to replace the non-sustainable and non-biocompatible electrically conductive polymers. For this, highly intrinsic conductive fillers can be dispersed within the biopolymeric matrices allowing to create a percolation pathway to improve the intrinsic conductivity of the biopolymer (Xiong et al., 2018; Zueva et al., 2020). Some studies combine electrically conductive carbon-based materials with the polysaccharides, namely carbon nanotubes (Castrejón-Parga et al., 2015; Montalbán, 2020), graphene oxide (Ma et al., 2012) and/or reduced graphene oxide (rGO) (Barra et al., 2019), but the interactions of rGO on starch/chitosan blended films have not yet been studied, at least to the best of our knowledge.

Pulsed electric field (PEF) is a non-thermal technology used to sterilize food products at low temperatures, maintaining their quality and extending their shelf-life (Pascall, 2018; Roodenburg et al., 2010). However, to avoid the costs of hygienic lines and machines as well as the re-contamination of the food after processing, this technology requires a food-grade packaging material to sterilize in-pack food products. Thus, a material with electrical conductivity is needed to allow the electrical current to pass through it, achieving the food product and inactivating the microorganisms and enzymes.

Biobased thermoplastic materials with suitable electrical conductive and active functional properties for food preservation demand further developments for technological application. To the best of our knowledge, the food compatible biobased composite materials do not fulfil the compromise of having, all together in just one material, a level of electrical conductivity in the order of 0.1–2 S/m for low temperature sterilization by PEF, while possessing mechanical strength for enabling extrusion, thermoplasticity for sealing, and bioactive antioxidant properties to enhance food shelf-life. Here, it is reported a study on the preparation of chitosan:starch blends with different ratios of each polysaccharide and the addition of reduced graphene oxide (rGO). The effect of blending and of the addition of rGO on the thermoplasticity of starch was followed by studying the sealing ability of the films. In addition it was investigated the mechanical properties, antioxidation properties, water wettability of the films' surface and electrical conductivity as the modifications were implemented.

2. Materials and methods

2.1. Materials

Commercial potato starch, provided by Sigma-Aldrich (St. Louis, MO, USA), contains approximately 73% of amylopectin and 27% of amylose, which corresponds to an amylopectin/amylose ratio of 2.7 (Gonçalves et al., 2020). Chitosan from shrimp shells of medium molecular weight (150 kDa) and with a deacetylation degree of 88% was supplied by Sigma-Aldrich (St. Louis, MO, USA). With a purity of 95%, this polysaccharide is also composed of alkali-soluble material (17%) and water-soluble material with a molecular weight lower than 12–14 kDa (6,2%) (Rocha et al., 2021). Graphite (~150 μm flakes), H_3PO_4 (≥85%), H_2SO_4 (97%), HCl (37%), $KMnO_4$ (99.0%), and H_2O_2 (30%) were purchased from Sigma-Aldrich Co (St. Louis, MO, USA). Glycerol (95%) was supplied from Scharlab, S.L. (Barcelona, Spain).

2.2. Synthesis of reduced graphene oxide

A modified methodology described by Marlinda et al. (2012) was used to produce rGO. The starting material was 20 mL of graphene oxide (GO) solution (6.6 mg/mL) prepared using the simplified Hummers method (Marcano et al., 2010). To this solution, 2 mL of 25% $NH_3{\cdot}H_2O$ with 0.354 g of NaOH were added and the mixture was stirred in a water bath at 60 ± 2 °C for 10 min until a cloudy dark brown liquid was obtained. Subsequently, the solution was transferred to a Teflon-lined stainless-steel autoclave (50 mL) and subjected to hydrothermal treatment for 24 h at 180 °C. The final rGO particles were obtained by washing with distilled water and ethanol until neutral pH and were suspended in a known amount of distilled water using a sonication tip of 3 mm (SONOPLUS HD 3100, 45 W, 20 min, pulse 10 s and pause 5 s) to determine its concentration for further use.

2.3. Preparation of starch/chitosan blend films reinforced with reduced graphene oxide

Each polysaccharide solution was prepared separately. Chitosan powder was mixed overnight at room temperature in distilled water with 0.1 M of acetic acid. Potato starch was dispersed in distilled water under magnetic agitation and gelatinized at 95 °C for 30 min in a thermostatic bath. Both polysaccharide solutions were thermostated at 50 °C and different mass fractions of starch and chitosan, specifically 75:25, 50:50, and 25:75, were blended to obtain a final solution with 1.5% (*w/v*). After 10 min of agitation at 50 °C for a homogeneous solution mixing, rGO suspension (25% *w*/w of dry polysaccharide blend weight) was added to the blend solutions. Glycerol (30% w/w of dry polysaccharide blend weight) was then added after 15 min, as plasticizer, and mixed under magnetic stirring for 10 min at 50 °C. The blend solutions were degassed under vacuum and a controlled weight (31 g) of each blend solution was transferred onto 144 cm^2 plexiglass plates of 3 mm deep. Neat starch film, neat chitosan film, and neat blended films (starch:chitosan at the proportion of 75:25, 50:50, and 25:75 *w*/w) with glycerol (30% *w*/w of dry polysaccharide weight), were made as control films. Additionally, control starch and chitosan films with rGO (25% w/w of dry polysaccharide weight) and glycerol (30% w/w of dry polysaccharide weight) were also produced. The films were obtained by a solvent casting methodology where the plates were placed in an oven with air circulation to evaporate the solvent at 30 °C for 16 h. The films were peeled off from the plates and conditioned at 53% RH in a controlled relative humidity chamber for at least 5 days before proceeding to their characterization. Films were named according to the type of polysaccharide proportion, for example, blend film composed of 25% starch and 75% chitosan is named as S25:C75 and when rGO was added to the blend, the label became S25:C75_rGO.

2.4. Characterization of starch/chitosan blend film

2.4.1. Structural and morphologic characterization

The Fourier Transform Infrared (FTIR) spectra were acquired using a Golden Gate single reflection diamond attenuated total reflectance (ATR) system in a Bruker IFS-55 spectrometer. Spectra were recorded at the absorbance mode from 4000 to 400 cm^{-1} wavenumber (mid-infrared region) with a resolution of 4 cm^{-1}. Five replicates (64 co-added scans) were collected for each sample.

X-ray diffraction (XRD) was performed on a Panalytical Empyrean X-ray diffractometer with Cu-K_α radiation ($\lambda = 1.54178$ Å). Films were recorded in a reflection mode with a scanning angle from 5° to 70° 2θ. Raman spectroscopy was carried out using the Jobin Yvon T64000 instrument equipped with a laser operating at 441 nm as an excitation source wavelength laser.

The surface and cross-section morphology of the films were observed using a high-resolution scanning electron microscopy (SEM, SU-70 Hitachi microscope) operating at 4 kV and 13 mm of working distance. Carbon tape was used to fix the samples on the SEM specimen holder and sputter-coated with carbon.

2.4.2. Water solubility and wettability

The films solubility was determined according to the method described by Nunes et al. (2013). One square (4 cm^2) of film, previously weighted, was placed in 30 mL of distilled water (pH 6.5), containing sodium azide (0.02 (*w/v*)), at room temperature for 7 days with orbital agitation (80 rpm). Afterwards, the films were dried at 105 °C for 16 h, cooled in a desiccator containing phosphorous pentoxide until room temperature, and weighed. The solubility was determined by the percentage of weight loss of the film, on a dry weight basis, where initial film weight was corrected considering the initial film moisture. The analysis was carried out with three independent assays.

Water contact angle on the surface (wettability) of films (strips of 1 × 10 cm) was performed at room temperature using a sessile drop of 3 μL of ultrapure water dispensed on the film surface. An OCA instrument (Dataphysics) was used for the measurements and the contact angle of the drops was calculated based on the Laplace-Young method with an image analysis software (Dataphysics SCA20M4). At least ten droplets were measured for the down and up film surface, where down and up means the film surface that is in contact with the plexiglass plate and the air during the solvent casting, respectively.

2.4.3. Mechanical properties

According to the standard method (ASTM D 882-83), tensile tests of films were performed using a texture analyzer apparatus (model TA.XT*plus*C, Stable Micro Systems) equipped with fixed grips with an initial separation of 50 mm. Films were cut in strips of 70 × 10 mm, fixed on the grips and stretched at a constant crosshead speed of 0.5 mm/s. At least six samples of each film were tested. Mechanical properties, such as tensile strength, elongation at break, and Young's modulus were determined from stress-strain curves. The films' thickness was measured in three different points along the strip using a digital micrometer with ±0.001 mm accuracy (Mitutoyo Corporation, Japan).

2.4.4. Antioxidant activity – ABTS assay

A modification of the ABTS method was used to evaluate films' antioxidant activity (Nunes et al., 2013). Firstly, a solution of 7 mM ABTS was prepared in 2.45 mM potassium persulfate and kept in dark at room temperature for 16 h, allowing the $ABTS^{\bullet+}$ formation. The $ABTS^{\bullet+}$ solution was diluted in water or ethanol (1:80) and its concentration was adjusted to 0.7–0.8 absorbance values measured at 734 nm (Powerwave HT, BioTek spectrophotometer microplate reader). One film square (1 cm^2) was placed in 3 mL of diluted $ABTS^{\bullet+}$ solution and left to react under dark conditions at room temperature with orbital stirring (80 rpm) over 24 h. The differences in absorbance to the blank allowed us to calculate the $ABTS^{\bullet+}$ inhibition percentage during the incubation time. $ABTS^{\bullet+}$ solution without film was used as blank. All measurements were performed in triplicate.

2.4.5. Electrical conductivity measurements

Films' electrical conductivity was evaluated in-plane and through-plane of the film using a homemade resistivity setup prepared with a 4-point probe and 2-point probe, respectively (Hiremath et al., 2006). Three strips (0.5 × 3.5 cm) of each film were cut to carry out the in-plane measurements and three squares (1 cm^2) of each film were cut for the through-plane assays. The electrical response was made at room temperature by direct current (*dc*) measurements using a programmable power supply IPS603 (ISO-Tech) and a Multimeter 34401A (HP). The value of electrical conductivity (S/m) for each film was then measured following Eqs. (1) and (2).

$$R = \frac{V}{I} \tag{1}$$

$$\sigma = \frac{L}{R \times A} \tag{2}$$

where R is the resistance, *V* means tension, I is current, σ is the electrical conductivity, L and A are the lengths and the cross-sectional area for each specimen.

2.4.6. Seal strength

To prepare the sealed film sample, two film pieces measuring 45 × 10 mm were placed on top of one another and sealed with a heat gradient tester. The sealing area was 10 × 10 mm^2 and occurred with a temperature around 140 °C for 5 s. Each sealed film was conditioned at 53% RH in a controlled relative humidity chamber for at least 48 h before the test. The seal strength was determined using a texture analyzer (model TA.XT*plus*C, Stable Micro Systems) according to the standard test method of ASTM F-88, with slight modifications (American Society for Testing and Materials, 2005). Samples were clamped to the instrument where the end of the sealed film was fixed perpendicularly to the test direction and placed in the center of the grip separation. The distance between the clamps was 50 mm and the loading speed was set as 1.5 mm/s. The seal strength was calculated using three replicas and following Eq. (3):

$$\textit{Seal strength}\ (\mathrm{N/mm}) = \frac{\textit{Peak force}\ (\mathrm{N})}{\textit{Film width}\ (\mathrm{mm})} \tag{3}$$

2.5. Statistical analysis

The results of solubility, surface wettability, mechanical properties, antioxidant activity, electrical conductivity, and seal strength were statistically evaluated using the analysis of variance (ANOVA) procedure in SPSS (trial version 24, SPSS Inc., Chicago, IL0 software). Tukey's Honestly Significant Difference (HSD) was used at the 95% confidence level to detect differences among mean values of films properties.

3. Results and discussion

Blended films of starch and chitosan with the rGO incorporation were developed to combine the thermoplastic behaviour of starch, the functional properties of chitosan, and the electrical conductivity and reinforcing potential of rGO. The pristine blended films demonstrated to be macroscopically homogenous and transparent, independently of the polysaccharide proportion. However, the addition of rGO turned the blended starch-chitosan films into a blackish colour while maintaining good homogeneity without phase separation.

3.1. Characterization of blended starch/chitosan-based films

3.1.1. Structural and morphological characterization

The ATR-FTIR analysis was performed to detect possible interactions between the starch and chitosan chains as well as with rGO filler and the spectra are shown in Fig. 1a. For the pristine starch film, the broadband at 3285 cm^{-1} is the signature band of the O—H stretching vibrations, whereas the bands at 1642 cm^{-1} and 1411 cm^{-1} are assigned to the O—H bending of bound water and CH_2, respectively. The bands at 1150 cm^{-1} and 994 cm^{-1} are attributed to the stretching vibration of C—O in C—O—H groups and C—O—C groups, respectively. In the spectrum of pristine chitosan film, the broadband from 3600 to 3100 cm^{-1} is attributed to the stretching vibration of N—H and O—H, respectively. The peaks located at 1639 cm^{-1}, 1551 cm^{-1}, and 1321 cm^{-1} are associated with amide I, amide II, and amide III, respectively. For both polysaccharides, peaks near 2930 cm^{-1} correspond to the C—H bond stretching vibrations of the methyl groups (—CH_2) (Ma et al., 2012; Ren et al., 2017). The different mass fractions of starch and chitosan in the blends led to changes in the characteristic spectrum bands of each polysaccharide. The addition of the highest amount of chitosan shows, as expected, the highest intensity of the functional groups of chitosan, specifically amide I, amide II, and amide III. Moreover, the addition of rGO to the starch/chitosan matrix does not add any new vibration band to the spectrum but changes the amplitude of some bands, namely decreases the broadband at 3000–3300 cm^{-1} attributed to O—H stretching. This result probably occurs due to the formation of hydrogen bonds between the rGO and the polysaccharide chains, indicating the good miscibility between the matrices and the filler.

The XRD patterns of pristine control films and blended films with or without the rGO incorporation are represented in Fig. 1b. As observed, the pristine starch film has one peak at $2\theta = 17.2°$ related to small regions of residual B-type crystallinity of potato starch granules, a second peak at $2\theta = 19.7°$ characteristic of *V*-type crystalline structure of glycerol interaction with starch chains during the gelatinization process, and the third one around $2\theta = 21.7°$ resultant of the dehydration of V-type crystallinity (Domene-López et al., 2019). The diffractogram of pristine chitosan film exhibits three main broad crystalline peaks around $2\theta = 9.4°$, 11.8°, and 20.8°, which represent its fingerprint and agrees with other reports (Suriyatem et al., 2018). After the blending of these two biopolymers, the crystallization pattern of starch is modified with the increased amount of chitosan, leading to the presence of an intense broad peak at 2θ around 20.3–20.8°. While less mass fraction of chitosan does not promote significant structural changes on the starch crystalline pattern, the higher amount of chitosan changes the crystalline regularity of each polysaccharide. This can indicate the formation of intermolecular interactions between the two polymers, which results in good compatibility and miscibility of the starch and chitosan matrices. Similar observations were also reported by other authors (Suriyatem et al., 2018). For comparison purposes, XRD pattern of rGO is displayed at the supplementary information (SI) (Fig. S1 at SI), where it is observed that the XRD reflections of rGO appear at the diffraction angles 2θ of 25.4° and 42.9°, which correspond to the (002) and (100) planes, respectively (Alves et al., 2021). These reflections are related with the disordered of graphite crystallites formed during the reduction reaction. When rGO is added to blended film, two broad bands are observed at 2θ around 8.4–9.4° and 20.9° for the films with the proportions of 75:25 and 50:50 of starch:chitosan, while at the highest mass fraction of chitosan, another peak related to the chitosan appears at 2θ around 11.6°. The XRD pattern profile of the blended films with rGO is mostly like the pristine chitosan film, but the bands have less intensity. Moreover, the peaks related to the starch disappear in the blended films with rGO, independently of the starch ratio. This may be related to a decrease in amylose-glycerol complexes formation due to the interactions of amylose with the graphene functional groups. However, it should be noted that the XRD pattern profile of blended films with rGO is very distinct from the neat blended film. This observation agrees with FTIR data, indicating that rGO can establish hydrogen bonds with the polysaccharides and hinders mobility, thus an ordered structure is formed along the rigid template offered by rGO (Chen et al., 2020). Additionally, the absence of the characteristic peaks of rGO sheets on the XRD

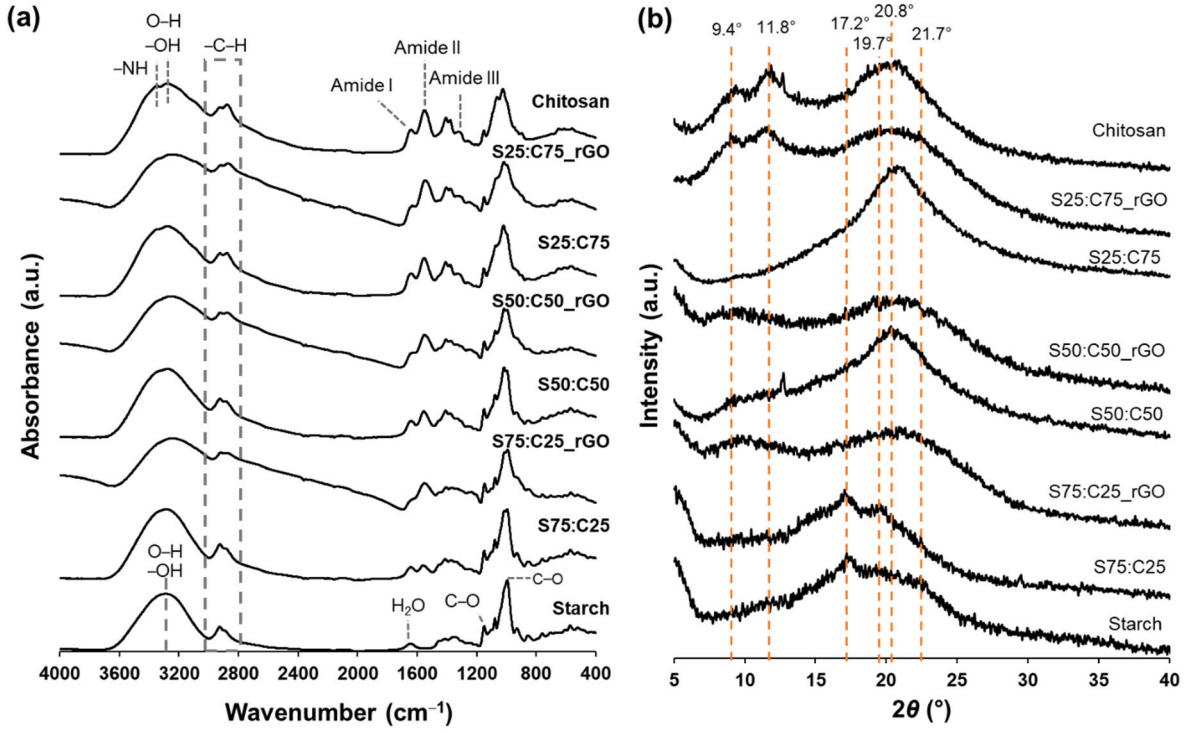

Fig. 1. (a) ATR-FTIR spectra and (b) X-ray diffraction patterns of pristine control films (starch and chitosan) and neat blend films with or without the addition of rGO.

patterns of blended films can indicate that most RGO sheets were exfoliated and uniformly dispersed in the biopolymer matrices, as observed by other authors (X. Wang et al., 2010).

The Raman spectra of rGO, pristine control films and blend films with rGO are represented in Fig. 2. Raman spectroscopy analysis is helpful to evaluate the structural properties of rGO filler after being added into the blends. The control starch film shows a prominent peak at 2920 cm^{-1} arising due to the stretching (C—H) of the alkyl groups (Peidayesh et al., 2020), while the control chitosan film does not show evidenced peaks in the spectrum. The obtained rGO shows a D band at 1368 cm^{-1} and a G band at 1592 cm^{-1}. The first one is characteristic of sp^3 disorder-induced carbon atoms and the second one represents the in-phase vibration of sp^2-bonded carbon atoms and is attributed to the crystalline graphitic plane (Ferrari & Basko, 2013). The ratio of D to G band equals to 1.80, indicating that the reduction of GO was not fully completed and that rGO remains with small structural defects, as oxygen-functional groups. Additionally, it is observed at 2963 cm^{-1} a weak band which represents the D + G band splitted from 2D, suggesting that rGO is composed of a multilayer structure. When rGO is incorporated into the polysaccharide matrix, the two characteristic bands of graphitic materials (D and G bands) are present in the blended film samples obtained with the different polymeric mass fractions, with a slight upward shift of the G band, which means interaction of rGO with the polysaccharide's chains. Indeed, the incorporation into the polysaccharide matrices increases the rGO crystallinity level since the I_D/I_G ratio is decreased (1.39, 1.40, and 1.40 for the S25:C75_rGO, S50:C50_rGO, and S75:C25_rGO, respectively). Consequently, with a more ordering structure the functional properties of rGO are maintained and are imparted to the starch/chitosan blends.

The polymer compatibility and the effect of rGO addition on the distinct starch-chitosan blended films were analysed by SEM (Fig. 3). The surfaces of the distinct starch-chitosan blended films (Fig. 3a) are smooth and uniform, however, changes in the surfaces occur after the rGO incorporation. The films containing rGO exhibit a rough morphology, identical to previous data reported in the literature (Barra et al., 2019). The cross-sectional images of neat blended films (Fig. 3b) indicate good compatibility between the two biopolymers, showing a continuous surface without pores or separation of phases. However, increasing the mass fraction of the chitosan matrix a small increase of roughness is notorious, which corroborates the XRD data where structural changes were observed due to different rearrangements of polymeric matrices. Moreover, the rGO addition enhances the surface roughness with a wave-like morphology, but the filler particles are homogeneously dispersed and well embedded throughout the biopolymer matrices (Fig. S2). This wave-like morphology is the result of interactions between the polymeric chains and the oxygen functional groups of rGO and are aligned parallel to the plexiglass plate used during solvent casting.

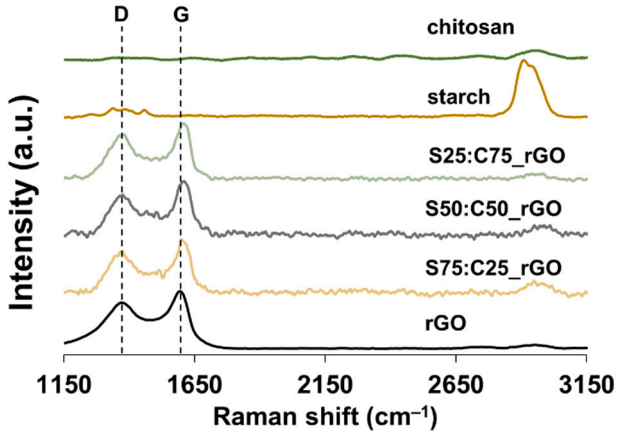

Fig. 2. Raman spectra of rGO, pristine control film (starch and chitosan), and the three different starch/chitosan blends with rGO incorporation.

3.1.2. *Wettability and solubility of starch/chitosan-based films*

The surface wettability of the films is one of the most important features when considering the use of these materials to packaged water-rich food products. The wettability property was investigated by water contact angle (WCA) measurements and the results are shown in Fig. 4a. The WCA of starch-chitosan blended films is in general above ~100°, suggesting a notable improvement of surface hydrophobicity in comparison with the pure starch film (46°). This observation, which is in agreement with the literature (Bangyekan et al., 2006; Luchese et al., 2018), occurs probably due to the hydrophobic surface nature of chitosan film which has a WCA value of 105°. It should be noted that only the presence of 25% of chitosan in the blended film is enough to increase about 2.3 times the hydrophobicity and to have similar behaviour to the surface of the pure chitosan film. In addition, the surface wettability does not show variability according to the different proportions of each polysaccharide. This leads to hypothesize that the NH_2 groups of chitosan establish a strong interaction with the —OH groups of starch chains by hydrogen bonds, decreasing the availability of these free hydrophilic groups to interact with the water molecules (Bangyekan et al., 2006). Moreover, the WCA of both sides of the film has not a significant difference that demonstrates the homogeneity of the film and the good mixture of the polysaccharides. Moreover, no considerable differences occur in the wettability of starch-chitosan blended films with the addition of rGO, contrary to what was reported by other authors that mention a decrease in WCA possibly due to the addition of rGO, since it increases the roughness of the film changing the materials' surface (Jabbari et al., 2019; Kosowska et al., 2018, 2019). As it can be seen in the SEM micrographs, the roughness of starch-chitosan based films is increased with the presence of rGO, but the strong intermolecular interaction between the two polysaccharides by hydrogen bonds increases the films' cohesion and seems to be crucial to maintain the hydrophobicity of the control blended films. Therefore, it is concluded that chitosan could provide an adequate hydrophobicity to the starch-chitosan blended films for a food packaging application.

Regarding the water solubility (Fig. 4b), this parameter was measured by the films' weight loss in distilled water for 7 days, indicating the films' water resistance. The solubility of blended films in water increases by adding a higher amount of chitosan. This occurs because pristine chitosan film shows to be more soluble in water (weight loss of 31%) than pristine starch film (weight loss of 23%), which is in agreement with the literature (Ren et al., 2017). Mostly of the weight loss probably occurs due to the diffusion of hydrophilic glycerol molecules, added as a plasticizer, from the films when immersed in the water medium (Nunes et al., 2015). The susceptibility to water is drastically reduced by adding rGO to the blended films, reaching a value of around 5–10% of weight loss. This lower solubility of biocomposite blended films could be attributed to the high hydrophobic nature of rGO, which exhibit less affinity to water (Etmimi et al., 2013). Additionally, the polar groups of both polysaccharides can interact through hydrogen bonds with the remaining oxygen-functional groups of rGO, giving the polysaccharide matrix lower accessibility or exposure to interact with water molecules (Shahbazi et al., 2017). The presence of rGO maintains the structural integrity of the films, enhancing their water resistance and the potential for a food packaging application.

3.1.3. *Mechanical properties*

Tensile tests were performed to understand the effect of polysaccharide proportions and addition of rGO on the films' mechanical properties, namely evaluated by the tensile strength (TS), Young's modulus (YM), and elongation at break (EB) parameters (Fig. 5). Pristine chitosan film had significant higher TS than the pristine starch film, whose values were 38.6 ± 4.0 MPa and 27.7 ± 3.1 MPa, respectively (Fig. 5a). However, the TS parameter did not significantly change with

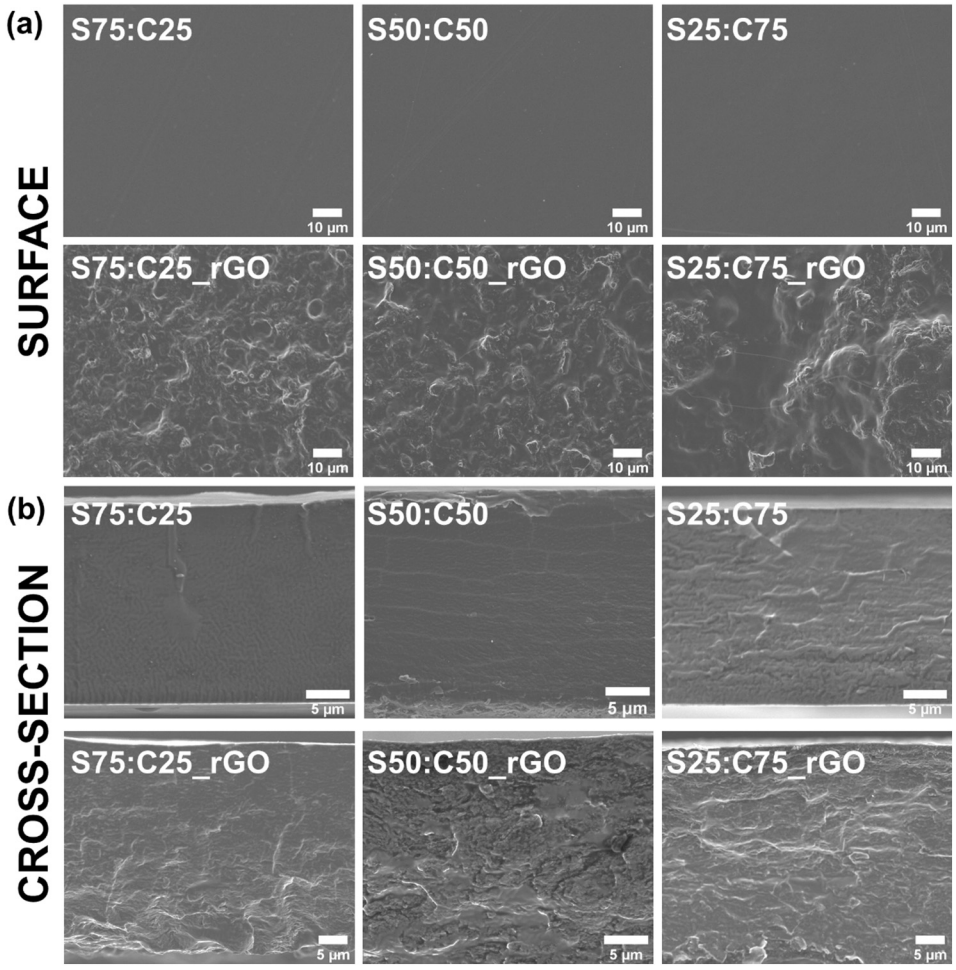

Fig. 3. (a) Surface and (b) cross-section micrographs of neat starch-chitosan blended films and blends with the incorporation of rGO.

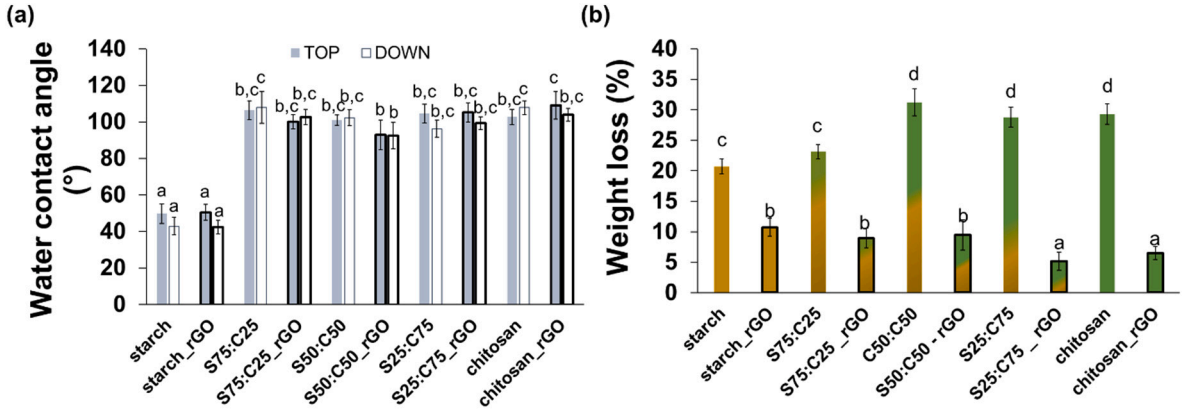

Fig. 4. (a) Water contact angle (WCA) of top and down surfaces (relatively to the cast mould) of pristine starch and chitosan films, and starch/chitosan blended films with or without rGO. (b) Water solubility (weight loss (%)) of the pristine and blended films of starch and chitosan with or without the presence of rGO. Bars with a black border represent the blended films with the rGO incorporation. Different letters represent significant ($p < 0.05$) values ($n = 30$ for WCA and n = 3 for the water solubility).

an increased proportion of chitosan in the starch matrix and not even with the addition of rGO filler. On the other side, increasing the amount of chitosan on the neat blended films, from 25 to 50 and 75 wt%, the YM values significantly decreased from 1.1 GPa (S25:C75) to 0.8 (S50:C50) and 0.6 GPa (S25:C75) (Fig. 5b). However, the addition of rGO to the S50:S50 and S25:C75 blended films increased their YM to 1.2 and 1.1 GPa, respectively. Regarding the EB (Fig. 5c), increasing the mass fraction of chitosan on the neat blended films enhanced the EB values to 36.9 ± 7.2%, almost 11 times more concerning the pristine starch film (3.4 ± 0.8%). However, this parameter was considerably decreased when the rGO was added to the blended films, demonstrating elongation values of less than 7%.

The mechanical performances indicate that increasing the proportion of chitosan on the blended starch-based film gives rise to materials

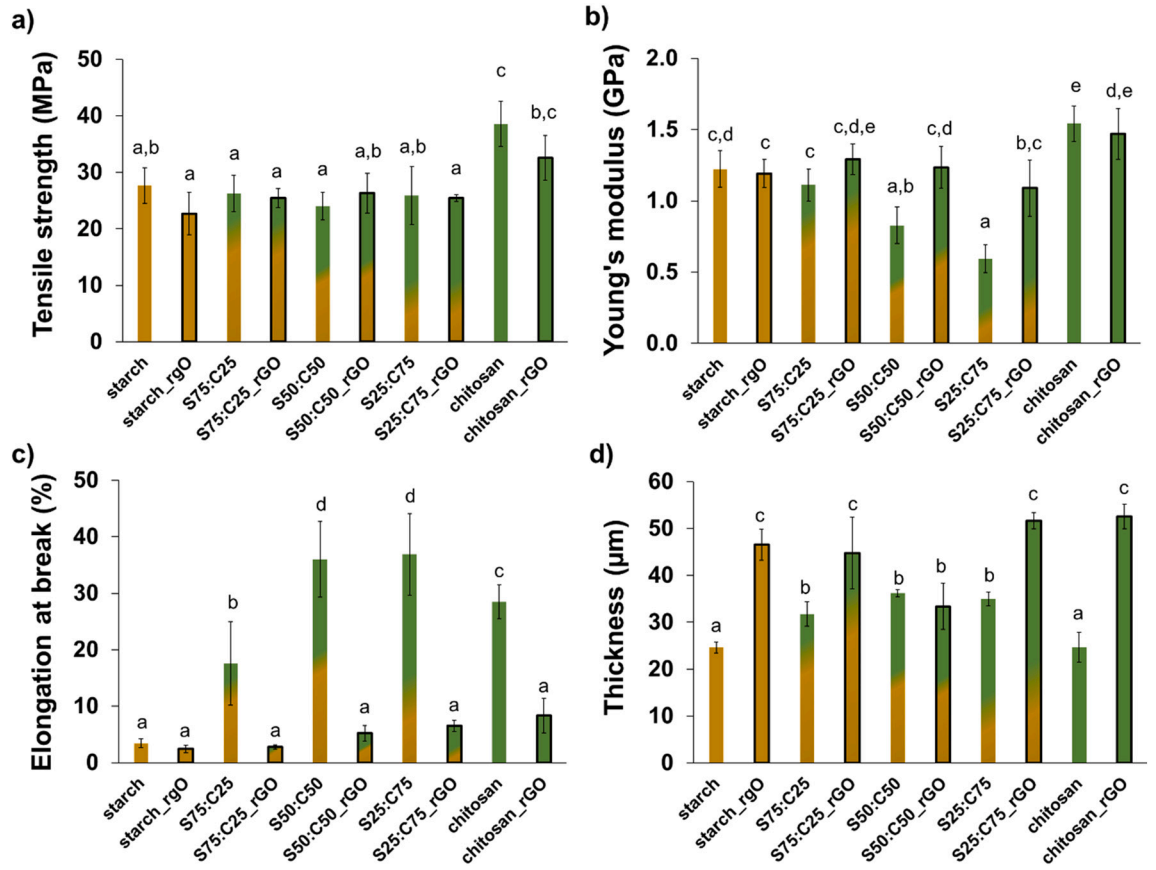

Fig. 5. Tensile strength (a), Young's modulus (b), elongation at break (c), and thickness (d) of the pristine and blended films derived from starch (yellow) and chitosan (green) with or without the presence of rGO. Bars with a black border represent the blended films with the rGO incorporation. Different letters represent significant ($p < 0.05$) values ($n = 6$). (For interpretation of the references to colour in this figure legend, the reader is referred to the web version of this article.)

with improved elasticity and stretchability. Thus, according to other reports, the chitosan matrix has plasticizing capacity (Merino & Alvarez, 2020; Pelissari et al., 2009). This occurs as a result of the interaction between starch and chitosan chains by hydrogen bonds, instead of intramolecular interactions of each polysaccharide, which allow an increase of biopolymeric chains mobility. This result agrees with the XRD pattern that demonstrates the perturbation of an otherwise orderly arrangement of pristine control films with the presence of the highest ratio of chitosan (Ren et al., 2017). As the blending process allows the increase of polymeric chains mobility, the blended films are less dense, increasing the films' thickness (Fig. 5d). In turn, the rGO addition turns the blended films with higher stiffness and decreased stretchability. The interaction of this stiff graphene-based material with the biopolymeric chains by hydrogen bonding, due to the presence of remaining oxygen-comprising groups on the surface of rGO sheets, restricts the mobility of blended polysaccharides and, thus, rGO acts as a reinforcing agent, in line with other studies (Barra et al., 2019; Yadav et al., 2013). Although the blended films turn less flexible with rGO, they are still manageable and highly suitable for food packaging applications.

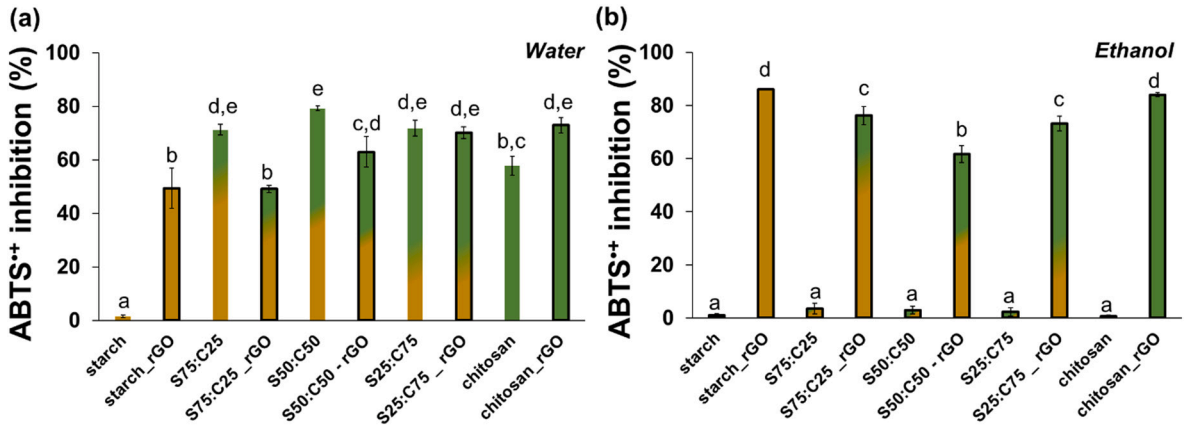

Fig. 6. Antioxidant activity of the pristine and blended films of starch (yellow) and chitosan (green) with or without the presence of rGO measured by ABTS method, using water (a) or ethanol (b) as a solvent. Bars with a black border represent the blended films with the rGO incorporation. Different letters represent significant ($p < 0.05$) values ($n = 3$). (For interpretation of the references to colour in this figure legend, the reader is referred to the web version of this article.)

3.1.4. Antioxidant activity

The antioxidant activity of all films was measured by the ABTS method in two different solvents, water (Fig. 6a) and ethanol (Fig. 6b). Using water as a solvent, the pristine starch film shows a radical inhibition around 1.5% for 4 h of contact while pristine chitosan film has a higher inhibition to around 58%. The antioxidant effect of chitosan films was also reported and occurs due to the ability of free amino groups (—NH_2) to react with free radicals to form a stable macromolecule with ammonium groups (—NH_3^+) via reaction with hydrogen ions from the solution (Avelelas et al., 2019; Ruiz-Navajas et al., 2013). The incorporation of rGO significantly increases the antioxidant activity of both pristine films, in accordance with the literature (Alves et al., 2021). Interestingly, the antioxidant activity of blended films is significantly higher than the pristine chitosan, reaching an inhibition ranging from 71% to 79%. As explained above, blending the polymers increases the mobility of polysaccharide chains and turns the films less dense. Thus, the amino groups are more available to interact with the ABTS radicals as well as their diffusion within the polymers to reach the amino groups is facilitated. The addition of rGO filler to the blended films slightly reduces the values of antioxidant activity when compared with the neat blended films probably due to the hydrophobic nature of rGO. This rGO feature can hinder the ABTS radical diffusion and reduce the availability of chitosan amino groups. In addition, a direct correlation of antioxidant activity enhancement with the chitosan mass fraction increment is shown in the blended films with rGO. Therefore, the blended film with a higher proportion of chitosan showed the highest antioxidant activity and the incorporation of the rGO maintains its activity.

When the ABTS radical was dissolved in ethanol, both the pristine films and the neat blended films showed a low inhibition for 7 h of reaction, less than 3.5%, due to the low solubility of hydrophilic chitosan polymer in ethanol. Nevertheless, the hydrophobic nature of rGO enables the blended films to have excellent antioxidant activity in ethanol, having the blended films with rGO inhibition of ABTS radical ranged from 62% to 76%, an increase over 20 times. The antioxidant activity of rGO was also reported in the literature and the scavenging activity is mainly associated with the radical adduct formation at sp^2 carbon network than the electron transfer or hydrogen donation of oxygen-containing functional groups (Qiu et al., 2014). Regardless of the type of food product to be packaged, whether it has a more hydrophobic or hydrophilic nature, these starch/chitosan blend films with the presence of rGO are the best choice due to their great advantage against oxidation.

3.1.5. Electrical conductivity

The electrical conductivity was measured by two approaches, in-plane (Fig. 7a) and through-plane (Fig. 7b) of the film. The in-plane electrical conductivity of pristine and neat blended films is less than 2.4×10^{-4} S/m, while the incorporation of rGO enables to increase this property but the improvement showed to be dependent on the polysaccharide mass fraction that comprises the blend. The starch film with rGO achieves the maximum electrical conductivity (6.51×10^{-3} S/m), followed by the blended one with the higher proportion of starch, S25:C75 (3.8×10^{-3} S/m). This trend is also confirmed in the through-plane electrical conductivity results, where the starch_rGO and S75:C25_rGO films had values of 2.9×10^{-6} S/m and 1.8×10^{-6} S/m, respectively. The other films with the rGO incorporation only reach through-plane conductivity values of around 10^{-7} S/m. In agreement with other reports, the in-plane conductivity is higher than the through-plane conductivity about 3 orders of magnitude, due to the preferential orientation of rGO layers along the in-plane direction (Yousefi et al., 2012). In summary, the dispersion of rGO in a matrix composed mostly of starch allows obtaining bionanocomposite films that stand out from the rest of the blends, presenting higher conductivity values in one order of magnitude. The electrical conductivity of polymer composites is highly dependent on the filler dispersion within the polymer matrix. However, the best dispersion features do not necessarily lead to the highest conductive values, since by SEM analysis a good dispersion of rGO is observed in all the distinct starch/chitosan blends. The results suggest that the presence of the highest starch mass fraction leads to the formation of the best percolation pathways and, consequently, to the enhancement of the electrical conductivity of the bionanocomposite. Increasing the amount of chitosan on blended films results in lower values of electrical conductivity possibly because this polysaccharide can interact with the rGO layers, establishing ionic linkages between the NH_3^+ groups and the free hydroxyl/carboxyl groups, preventing the direct contact among the rGO sheets and the formation of a conductive network (Cobos et al., 2018). Still, increasing the mass fraction of rGO up to 50% of the total dry polysaccharide weight may be of interest to obtain superior electrical conductivity on the starch/chitosan blended films, as observed on the polysaccharide-based films of previous studies with rGO addition (Alves et al., 2021; Barra et al., 2019).

3.1.6. Heat seal strength

The evaluation of the heat sealability is an important factor, from a technological point of view, for the packaging application of these films. The effect of mixing chitosan and rGO on seal strength of starch-based films were evaluated for pristine starch, starch_rGO, S75:C25, S75:C25_rGO, S25:C75, and S25:C75_rGO (Fig. 8). The results show that pristine starch film has a seal strength of 0.06 N/mm sealed at 140 °C, which is a quite low value when compared with the literature (≈0.30 N/mm) (Rompothi et al., 2017; Sadegh-Hassani & Mohammadi Nafchi, 2014) probably due to the lower final polymeric concentration (1.5%) of

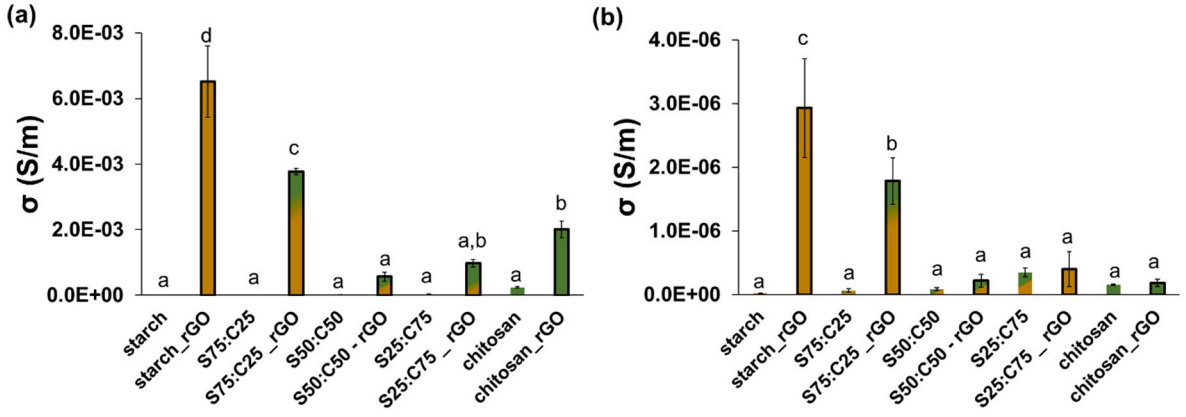

Fig. 7. (a) In-plane and (b) through-plane electrical conductivity of the pristine and blended films derived from starch (yellow) and chitosan (green) with or without the presence of rGO. Bars with a black border represent the blended films with the rGO incorporation. Different letters represent significant ($p < 0.05$) values ($n = 3$). (For interpretation of the references to colour in this figure legend, the reader is referred to the web version of this article.)

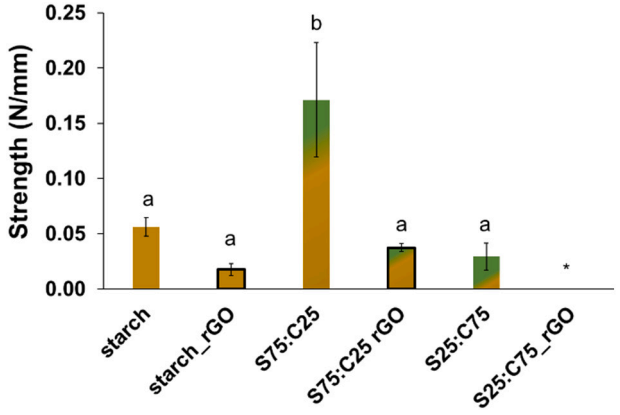

Fig. 8. Effect of chitosan (green) mass fraction and rGO addition on heat seal strength of starch-based films (yellow). Bars with a black border represent the films with the rGO incorporation. * - 25S:75C_rGO film does not show sealability. Different letters represent significant ($p < 0.05$) values ($n = 3$). (For interpretation of the references to colour in this figure legend, the reader is referred to the web version of this article.)

the films here studied, and consequently, less starch quantity to be melted. On the other hand, the combined addition of 75% of starch with 25% of chitosan led to the highest seal strength (0.17 N/mm) obtained in this study, indicating that this mass fraction of chitosan acts as a plasticizer, helping to enhance the molecular interdiffusion during the sealing. This polymeric reassociation occurs mainly via hydrogen bonding between the polymeric chains, but also with the hydroxyl groups of glycerol molecules. A full combination of these interactions enables the highest elongation at break which causes the best melting and hence the improved sealing behaviour. However, by increasing the chitosan proportion in the blend the heat seal strength decreases because of the lack of thermoplasticity of the chitosan matrix which cannot be directly melted (Grande et al., 2018; Matet et al., 2014).

The addition of rGO also demonstrates a great impact on the seal strength, decreasing the force required for separating films from each other to a strength inferior to 0.04 N/mm. Compared to S25:C75 blended film, the rGO impedes even the films' sealability. As observed by the low elongation at break, the presence of rGO on the blend restricts the mobility of the polymeric chains. Subsequent, the hydrogen bonding contact between the two polysaccharides decreases and affects the main forces responsible for the films' sealability. In general, all the films have a detachment of the adhesive sealed regions (peeling mode failure) and this type of failure mode occurs usually when the polymer films were sealed at a temperature substantially lower than their melting point. This is under other authors studies, which demonstrates a peeling mode failure when corn starch-based films containing a functional polysaccharide (amylose, methylcellulose or hydroxypropylmethylcellulose) were sealed below 143 °C (Das & Chowdhury, 2016). The mode of failure indicates the quality of heat sealing, but also suggest the opening mode of the sealed package. When the seal strength has a high value, the sealed package has a greater ability to resist separation or seal tearing, in turn, a low value of seal strength can be required to have a sealed package with an easy-peel opening (Farhan & Hani, 2017; Voon et al., 2012).

4. Conclusion

The films production of blends of thermoplastic potato starch and antioxidant chitosan matrix was performed by solvent casting, varying the mass fraction of each polymer and also with the addition of 25 wt% of rGO. Aiming a food packaging material with active properties and electrical conductivity, the bionanocomposite with higher potential was the one developed with 75% starch and 25% chitosan containing rGO. This lowest mass fraction of chitosan was effective to improve the surface hydrophobicity (>100°), maintaining the seal strength of starch-based films. Additionally, the incorporation of rGO allowed to obtain a blended film with better mechanical performance, water resistance, and electrical conductivity while maintain the seal strength similar to the neat starch-based film. Along with this, both chitosan and rGO were important to enhance the antioxidant activity of starch-based films in both water and ethanol, allowing a oxidative protection in a wider range of food products, which can have a hydrophilic or hydrophobic nature.

In sum, the food-grade bionanocomposite with electrically conductive properties may be an interesting alternative to conventional non-biodegradable plastics in the food packaging industry, potentially allowing the PEF treatment to sterilize in-pack food products, such as fruit and vegetable mashes or dairy products. Furthermore, the combination of this food treatment with the active properties of the starch/chitosan/rGO films helps to maintain the safety of packaged food for a longer time than common plastics.

CRediT authorship contribution statement

Zélia Alves: Investigation, Formal analysis, Writing – original draft, Visualization. **Nuno M. Ferreira:** Investigation, Writing – review & editing. **Paula Ferreira:** Conceptualization, Writing – review & editing, Supervision. **Cláudia Nunes:** Conceptualization, Writing – review & editing, Supervision.

Declaration of competing interest

The authors declare that they have no known competing financial interests or personal relationships that could have appeared to influence the work reported in this paper.

Acknowledgements

This work was developed within the scope of the project CICECO-Aveiro Institute of Materials, UIDB/50011/2020, UIDP/50011/2020 & LA/P/0006/2020, and i3N, UIDB/50025/2020 & UIDP/50025/2020, financed by national funds through the Fundação para a Ciência e a Tecnologia/ Ministério da Educação e Ciência (FCT/MEC) Programa de Investimentos e Despesas de Desenvolvimento da Administração Central (PIDDAC). ZA and PF thank FCT for the grants (PD/BD/117457/2016 and IF/00300/2015, respectively). This work was also supported by BIOFOODPACK project (M-ERA.NET2/0019/2016) and by national funds (OE), through FCT, I.P., in the scope of the framework contract foreseen in the numbers 4, 5 and 6 of the article 23, of the Decree-Law 57/2016, of August 29, changed by Law 57/2017, of July 19. The authors thank António Fernandes for his technical assistance with Raman measurements.

Appendix A. Supplementary data

Supplementary data to this article can be found online at https://doi.org/10.1016/j.carbpol.2022.119517.

References

Alves, Z., Ferreira, N. M., Mendo, S., Ferreira, P., & Nunes, C. (2021). Design of alginate-based bionanocomposites with electrical conductivity for active food packaging. *International Journal of Molecular Sciences, 22*, 9943.

American Society for Testing and Materials. (2005). Standard test method for seal strength of flexible barrier materials F88. In *Annual book of ASTM standards*.

Avelelas, F., Horta, A., Pinto, L. F. V., Marques, S. C., Nunes, P. M., Pedrosa, R., & Leandro, S. M. (2019). Antifungal and antioxidant properties of chitosan polymers obtained from nontraditional Polybius henslowii sources. *Marine Drugs, 17*(4), 1–15.

Bangyekan, C., Aht-Ong, D., & Srikulkit, K. (2006). Preparation and properties evaluation of chitosan-coated cassava starch films. *Carbohydrate Polymers, 63*(1), 61–71.

Barra, A., Ferreira, N. M., Martins, M. A., Lazar, O., Pantazi, A., Jderu, A. A., Neumayer, S. M., Rodriguez, B. J., Enăchescu, M., Ferreira, P., & Nunes, C. (2019). Eco-friendly preparation of electrically conductive chitosan - reduced graphene

oxide flexible bionanocomposites for food packaging and biological applications. *Composites Science and Technology, 173*(November 2018), 53–60. https://doi.org/10.1016/j.compscitech.2019.01.027

Castrejón-Parga, K. Y., Camacho-Montes, H., Rodríguez-González, C. A., Velasco-Santos, C., Martínez-Hernández, A. L., Bueno-Jaquez, D., Rivera-Armenta, J. L., Ambrosio, C. R., Conzalez, C. C., Mendoza-Duarte, M. E., & García-Casillas, P. E. (2015). Chitosan-starch film reinforced with magnetite-decorated carbon nanotubes. *Journal of Alloys and Compounds, 615*(S1), S505–S510.

Ceballos, R. L., Ochoa-Yepes, O., Goyanes, S., Bernal, C., & Famá, L. (2020). Effect of yerba mate extract on the performance of starch films obtained by extrusion and compression molding as active and smart packaging. *Carbohydrate Polymers, 244* (December 2019), Article 116495.

Chen, P., Xie, F., Tang, F., & McNally, T. (2020). Glycerol plasticisation of chitosan/carboxymethyl cellulose composites: Role of interactions in determining structure and properties. *International Journal of Biological Macromolecules, 163*, 683–693. https://doi.org/10.1016/j.ijbiomac.2020.07.004

Chotiprayon, P., Chaisawad, B., & Yoksan, R. (2020). Thermoplastic cassava starch/poly (lactic acid) blend reinforced with coir fibres. *International Journal of Biological Macromolecules, 156*, 960–968.

Cobos, M., González, B., Fernández, M. J., & Fernández, M. D. (2018). Study on the effect of graphene and glycerol plasticizer on the properties of chitosan-graphene nanocomposites via in situ green chemical reduction of graphene oxide. *International Journal of Biological Macromolecules, 114*, 599–613.

Copeland, L., Blazek, J., Salman, H., & Tang, M. C. (2009). Form and functionality of starch. *Food Hydrocolloids, 23*(6), 1527–1534.

Das, M., & Chowdhury, T. (2016). Heat sealing property of starch based self-supporting edible films. *Food Packaging and Shelf Life, 9*, 64–68.

Domene-López, D., García-Quesada, J. C., Martin-Gullon, I., & Montalbán, M. G. (2019). Influence of starch composition and molecular weight on physicochemical properties of biodegradable films. *Polymers, 11*(7), 1084.

Etmimi, H. M., Mallon, P. E., & Sanderson, R. D. (2013). Polymer/graphite nanocomposites: Effect of reducing the functional groups of graphite oxide on water barrier properties. *European Polymer Journal, 49*(11), 3460–3470. https://doi.org/10.1016/j.eurpolymj.2013.08.004

Farhan, A., & Hani, N. M. (2017). Characterization of edible packaging films based on semi-refined kappa-carrageenan plasticized with glycerol and sorbitol. *Food Hydrocolloids, 64*, 48–58.

Ferrari, A. C., & Basko, D. M. (2013). Raman spectroscopy as a versatile tool for studying the properties of graphene. *Nature Nanotechnology, 8*(4), 235–246.

Ferreira, A. R. V., Alves, V. D., & Coelhoso, I. M. (2016). Polysaccharide-based membranes in food packaging applications. *Membranes, 6*(2), 1–17.

Ghanbarzadeh, B., Oleyaei, S. A., & Almasi, H. (2015). Nanostructured materials utilized in biopolymer-based plastics for food packaging applications. *Critical Reviews in Food Science and Nutrition, 55*(12), 1699–1723.

Gonçalves, I., Lopes, J., Barra, A., Hernández, D., Nunes, C., Kapusniak, K., Kapusniak, J., Evtyugin, D. V., Lopes, J. A., Ferreira, P., & Coimbra, M. A. (2020). Tailoring the surface properties and flexibility of starch-based films using oil and waxes recovered from potato chips byproducts. *International Journal of Biological Macromolecules, 163*, 251–259.

Grande, R., Pessan, L. A., & Carvalho, A. J. F. (2018). Thermoplastic blends of chitosan: A method for the preparation of high thermally stable blends with polyesters. *Carbohydrate Polymers, 191*(December 2017), 44–52.

Gürler, N., & Torğut, G. (2020). Graphene-reinforced potato starch composite films: Improvement of mechanical, barrier and electrical properties. *Polymer Composites, June*, 1–8.

Haghighi, H., Licciardello, F., Fava, P., Siesler, H. W., & Pulvirenti, A. (2020). Recent advances on chitosan-based films for sustainable food packaging applications. *Food Packaging and Shelf Life, 26*(July), Article 100551.

Hasan, M., Gopakumar, D. A., Olaiya, N. G., Zarlaida, F., Alfian, A., Aprinasari, C., Alfatah, T., Rizal, S., & Khalil, H. P. S. A. (2020). Evaluation of the thermomechanical properties and biodegradation of brown rice starch-based chitosan biodegradable composite films. *International Journal of Biological Macromolecules, 156*, 896–905.

Hiremath, R. K., Rabinal, M. K., & Mulimani, B. G. (2006). Simple setup to measure electrical properties of polymeric films. *Review of Scientific Instruments, 77*(12), 1–4.

Jabbari, F., Hesaraki, S., & Houshmand, B. (2019). The physical, mechanical, and biological properties of silk fibroin/chitosan/reduced graphene oxide composite membranes for guided bone regeneration. *Journal of Biomaterials Science, Polymer Edition, 30*(18), 1779–1802.

Junlapong, K., Boonsuk, P., Chaibundit, C., & Chantarak, S. (2019). Highly water resistant cassava starch/poly(vinyl alcohol) films. *International Journal of Biological Macromolecules, 137*, 521–527.

Kabir, E., Kaur, R., Lee, J., Kim, K. H., & Kwon, E. E. (2020). Prospects of biopolymer technology as an alternative option for non-degradable plastics and sustainable management of plastic wastes. *Journal of Cleaner Production, 258*, Article 120536.

Kong, R., Wang, J., Cheng, M., Lu, W., Chen, M., Zhang, R., & Wang, X. (2020). Development and characterization of corn starch/PVA active films incorporated with carvacrol nanoemulsions. *International Journal of Biological Macromolecules, 164*, 1631–1639.

Kosowska, K., Domalik-Pyzik, P., Krok-Borkowicz, M., & Chłopek, J. (2019). Synthesis and characterization of chitosan/reduced graphene oxide hybrid composites. *Materials, 12*(13).

Kosowska, K., Domalik-Pyzik, P., Nocuń, M., & Chłopek, J. (2018). Chitosan and graphene oxide/reduced graphene oxide hybrid nanocomposites – evaluation of physicochemical properties. *Materials Chemistry and Physics, 216*(May), 28–36.

Lim, W. S., Ock, S. Y., Park, G. D., Lee, I. W., Lee, M. H., & Park, H. J. (2020). Heat-sealing property of cassava starch film plasticized with glycerol and sorbitol. *Food Packaging and Shelf Life, 26*(July), Article 100556.

Luchese, C. L., Pavoni, J. M. F., dos Santos, N. Z., Quines, L. K., Pollo, L. D., Spada, J. C., & Tessaro, I. C. (2018). Effect of chitosan addition on the properties of films prepared with corn and cassava starches. *Journal of Food Science and Technology, 55*(8), 2963–2973.

Ma, J., Liu, C., Li, R., & Wang, J. (2012). Properties and structural sharacterization of oxide starch/chitosan/graphene oxide biodegradable nanocomposites. *Journal of Applied Polymer Science, 123*, 2933–2944.

Marcano, D. C., Kosynkin, D. V., Berlin, J. M., Sinitskii, A., Sun, Z., Slesarev, A., Alemany, L. B., Lu, W., & Tour, J. M. (2010). Improved synthesis of graphene oxide. *ACS Nano, 4*(8), 4806–4814. https://doi.org/10.1021/nn1006368

Marlinda, A. R., Huang, N. M., Muhamad, M. R., An'Amt, M. N., Chang, B. Y. S., Yusoff, N., Harrison, I., Lim, H. N., Chia, C. H., & Kumar, S. V. (2012). Highly efficient preparation of ZnO nanorods decorated reduced graphene oxide nanocomposites. *Materials Letters, 80*, 9–12. https://doi.org/10.1016/j.matlet.2012.04.061

Matet, M., Heuzey, M. C., & Ajji, A. (2014). Morphology and antibacterial properties of plasticized chitosan/metallocene polyethylene blends. *Journal of Materials Science, 49*(15), 5427–5440.

Merino, D., & Alvarez, V. A. (2020). Green microcomposites from renewable resources: Effect of seaweed (Undaria pinnatifida) as filler on corn starch–chitosan film properties. *Journal of Polymers and the Environment, 28*(2), 500–516.

Montalbán, M. G. (2020). Electroconductive starch/multi-walled carbon nanotube films plasticized by 1-ethyl-3-methylimidazolium acetate. *Carbohydrate Polymers, 229*, Article 115545.

Mose, B. R., & Maranga, S. M. (2011). A review on starch based nanocomposites for bioplastic materials. *Journal of Materials Science and Engineering, 1*, 239–245.

Nevoralová, M., Koutný, M., Ujčić, A., Starý, Z., Šerá, J., Vlková, H., Šlouf, M., Fortelný, I., & Kruliš, Z. (2020). Structure characterization and biodegradation rate of poly(ε-caprolactone)/starch blends. *Frontiers in Materials, 7*(June), 1–14.

Nunes, C., Maricato, É., Cunha, Â., Nunes, A., Lopes, J. A., & Coimbra, M. A. (2013). Chitosan – caffeic acid – genipin films presenting enhanced antioxidant activity and stability in acidic media. *Carbohydrate Polymers, 91*(1), 236–243.

Nunes, C., Maricato, É., Gonçalves, F. J., da Silva, J. A. L., Rocha, S. M., & Coimbra, M. A. (2015). Properties of chitosan-genipin films grafted with phenolic compounds from red wine. *Trends in Carbohydrate Research, 7*(1), 25–32.

Nzenguet, A. M., Aqlil, M., Essamlali, Y., Amadine, O., Snik, A., Larzek, M., & Zahouily, M. (2018). Novel bionanocomposite films based on graphene oxide filled starch/polyacrylamide polymer blend: Structural, mechanical and water barrier properties. *Journal of Polymer Research, 25*, 86.

Ojogbo, E., Ogunsona, E. O., & Mekonnen, T. H. (2020). Chemical and physical modifications of starch for renewable polymeric materials. *Materials Today Sustainability, 7–8*, Article 100028.

Pascall, M. A. (2018). Packaging for high-pressure processing, irradiation, and pulsed electric field. In M. A. Pascall, & J. H. Han (Eds.), *Packaging for nonthermal processing of food* (Second, pp. 95–119). John Wiley & Sons Ltd.

Peidayesh, H., Ahmadi, Z., Khonakdar, H. A., Abdouss, M., & Chodák, I. (2020). Fabrication and properties of thermoplastic starch/montmorillonite composite using dialdehyde starch as a crosslinker. *Polymer International, 69*(3), 317–327.

Pelissari, F. M., Grossmann, M. V. E., Yamashita, F., & Pineda, E. A. G. (2009). Antimicrobial, mechanical, and barrier properties of cassava starch-chitosan films incorporated with oregano essential oil. *Journal of Agricultural and Food Chemistry, 57*(16), 7499–7504.

Qiu, Y., Wang, Z., Owens, A. C. E., Kulaots, I., Chen, Y., Kane, A. B., & Hurt, R. H. (2014). Antioxidant chemistry of graphene-based materials and its role in oxidation protection technology. *Nanoscale, 6*(20), 11744–11755.

Ren, L., Yan, X., Zhou, J., Tong, J., & Su, X. (2017). Influence of chitosan concentration on mechanical and barrier properties of corn starch/chitosan films. *International Journal of Biological Macromolecules, 105*, 1636–1643.

Rocha, M. A. M., Coimbra, M. A., Rocha, S. M., & Nunes, C. (2021). Impact of chitosan-genipin films on volatile profile of wine along storage. *Applied Sciences (Switzerland), 11*, 6294.

Rompothi, O., Pradipasena, P., Tananuwong, K., Somwangthanaroj, A., & Janjarasskul, T. (2017). Development of non-water soluble, ductile mung bean starch based edible film with oxygen barrier and heat sealability. *Carbohydrate Polymers, 157*, 748–756.

Roodenburg, B., de Haan, S. W. H., van Boxtel, L. B. J., Hatt, V., Wouters, P. C., Coronel, P., & Ferreira, J. A. (2010). Conductive plastic film electrodes for pulsed electric field (PEF) treatment - a proof of principle. *Innovative Food Science and Emerging Technologies, 11*(2), 274–282.

Ruiz-Navajas, Y., Viuda-Martos, M., Sendra, E., Perez-Alvarez, J. A., & Fernández-López, J. (2013). In vitro antibacterial and antioxidant properties of chitosan edible films incorporated with thymus moroderi or thymus piperella essential oils. *Food Control, 30*(2), 386–392.

Sadegh-Hassani, F., & Mohammadi Nafchi, A. (2014). Preparation and characterization of bionanocomposite films based on potato starch/halloysite nanoclay. *International Journal of Biological Macromolecules, 67*, 458–462.

Shahbazi, M., Rajabzadeh, G., & Sotoodeh, S. (2017). Functional characteristics, wettability properties and cytotoxic effect of starch film incorporated with multi-walled and hydroxylated multi-walled carbon nanotubes. *International Journal of Biological Macromolecules, 104*, 597–605.

Suriyatem, R., Auras, R. A., & Rachtanapun, P. (2018). Improvement of mechanical properties and thermal stability of biodegradable rice starch–based films blended with carboxymethyl chitosan. *Industrial Crops and Products, 122*(May), 37–48.

Thakur, R., Pristijono, P., Scarlett, C. J., Bowyer, M., Singh, S. P., & Vuong, Q. V. (2019). Starch-based films: Major factors affecting their properties. *International Journal of Biological Macromolecules, 132*, 1079–1089.

Vedove, T. M. A. R. D., Maniglia, B. C., & Tadini, C. C. (2021). Production of sustainable smart packaging based on cassava starch and anthocyanin by an extrusion process. *Journal of Food Engineering, 289*(July 2020), Article 110274.

Voon, H. C., Bhat, R., Easa, A. M., Liong, M. T., & Karim, A. A. (2012). Effect of addition of halloysite nanoclay and SiO2 nanoparticles on barrier and mechanical properties of bovine gelatin films. *Food and Bioprocess Technology, 5*, 1766–1774.

Wang, W., Xue, C., & Mao, X. (2020). Chitosan: Structural modification, biological activity and application. *International Journal of Biological Macromolecules, 164*, 4532–4546.

Wang, X., Bai, H., Yao, Z., Liu, A., & Shi, G. (2010). Electrically conductive and mechanically strong biomimetic chitosan/reduced graphene oxide composite films. *Journal of Materials Chemistry, 20*(41), 9032–9036.

Weerapoprasit, C., & Prachayawarakorn, J. (2016). Properties of biodegradable thermoplastic cassava Starch/Sodium alginate composites prepared from injection molding. *Polymer Composites, 37*(12), 3365–3372.

Xiong, R., Grant, A. M., Ma, R., Zhang, S., & Tsukruk, V. V. (2018). Naturally-derived biopolymer nanocomposites: Interfacial design, properties and emerging applications. *Materials Science and Engineering R: Reports, 125*, 1–41.

Yadav, S. K., Jung, Y. C., Kim, J. H., Ko, Y. I., Ryu, H. J., Yadav, M. K., Kim, Y. A., & Cho, J. W. (2013). Mechanically robust, electrically conductive biocomposite films using antimicrobial chitosan-functionalized graphenes. *Particle and Particle Systems Characterization, 30*(8), 721–727.

Yousefi, N., Gudarzi, M. M., Zheng, Q., Aboutalebi, S. H., Sharif, F., & Kim, J. K. (2012). Self-alignment and high electrical conductivity of ultralarge graphene oxide-polyurethane nanocomposites. *Journal of Materials Chemistry, 22*(25), 12709–12717.

Zhang, Y., Rempel, C., & Liu, Q. (2014). Thermoplastic starch processing and characteristics - a review. *Critical Reviews in Food Science and Nutrition, 54*(10), 1353–1370.

Zheng, K., Xiao, S., Li, W., Wang, W., Chen, H., Yang, F., & Qin, C. (2019). Chitosan-acorn starch-eugenol edible film: Physico-chemical, barrier, antimicrobial, antioxidant and structural properties. *International Journal of Biological Macromolecules, 135*, 344–352.

Zueva, O. S., Gubaidullin, A. T., Makarova, A. O., Bogdanova, L. R., Zakharova, L. Y., & Zuev, Y. F. (2020). Structural features of composite protein-polysaccharide hydrogel in the presence of a carbon nanomaterial. *Russian Chemical Bulletin, 69*(3), 581–589.